Exploring Cuneanes as Benzene Isosteres and Energetic Materials: Scope and Mechanistic Investigations into Regioselective Rearrangements from Cubanes

Jeong-Yu Son[1], Santeri Aikonen[2], Nathan Morgan[3], Alexander S. Harmata[1], Jesse J. Sabatini[4], Rosario C. Sausa[5], Edward F. C. Byrd[5], Daniel H. Ess[3]*, Robert S. Paton[2]*, and Corey R. J. Stephenson[1]*

[1]Department of Chemistry, University of Michigan, Ann Arbor, Michigan 48109, United States

[2]Department of Chemistry, Colorado State University, Fort Collins, Colorado 80523, United States

[3]Department of Chemistry & Biochemistry, Brigham Young University, Provo, Utah 84602, United States

[4]US Army Research Laboratory, Energetics Technology Branch, Aberdeen Proving Ground, MD 21005, United States

[5]DEVCOM Army Research Laboratory, Energetics Simulation & Modeling Branch, Aberdeen Proving Ground, MD 21005, United States

ABSTRACT: Cuneane is a strained hydrocarbon accessible via metal-catalyzed isomerization of cubane. The carbon atoms of cuneane define a polyhedron of the C_{2v} point group with six faces- two triangular, two quadrilateral, and two pentagonal. The rigidity, strain, and unique exit vectors of the cuneane skeleton make it a potential scaffold of interest for the synthesis of functional small molecules and materials. However, the limited previous synthetic efforts towards cuneanes have focused on monosubstituted or redundantly substituted systems such as permethylated, perfluorinated, and bis(hydroxymethylated) cuneanes. Such compounds, particularly rotationally symmetric redundantly substituted cuneanes, have limited potential as building blocks for the synthesis of complex molecules. Reliable, predictable, and selective syntheses of poly-substituted cuneanes bearing more complex substitution patterns would facilitate the study of this ring system in myriad applications. Herein, we report the regioselective, Ag[I]-catalyzed isomerization of asymmetrically 1,4-disubstituted cubanes to cuneanes. In-depth DFT calculations provide a charge-controlled regioselectivity model and direct dynamics simulations indicate that the non-classical carbocation is short-lived and dynamic effects augment the charge model.
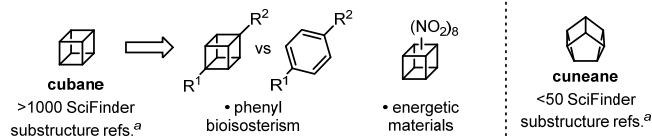
INTRODUCTION

Cubane has continuously inspired the chemical community since its synthesis was first reported by Eaton in 1964 due, in large part, to its beautiful symmetry, high strain energy, and impressive kinetic stability.[1] Consequently, cubane derivatives have been studied in a multitude of applications ranging from energetic materials to pharmaceuticals (Figure 1A).[2] Decades after publishing his seminal cubane synthesis, Eaton noted the similar exit vectors of 1,4-disubstituted cubanes and *para*-disubstituted benzene rings, leading him to propose cubane as a potential scaffold for drug development.[3] This hypothesis has stimulated further research comparing the performance and properties of benzene-derived and cubane-derived functional molecules in both biological and abiotic systems.[4, 5]

For all the attention cubane has received, relatively little has been given to its aliphatic hydrocarbon isomer, cuneane, despite its potential as a valuable molecular scaffold in its own right (Figure 1A).[6] The synthesis of cuneane was first reported by Eaton in 1970 and was achieved via the Ag[I]- or Pd[II]-catalyzed isomerization of cubane (Figure 1B).[7] Beyond preparing the parent compound, Eaton demonstrated the rearrangement with several mono- and *symmetrically* 1,4-disubstituted cubanes (Figure 1B and Figure 1C, respectively). The former gave mixtures of all three possible cuneane isomers, while the latter gave only two (of ten possible) substitution patterns (hereafter the "1,3- and 2,6-isomers"). Eaton attributed the selectivity for the 1,3- and 2,6-isomers over the eight other possible substitution
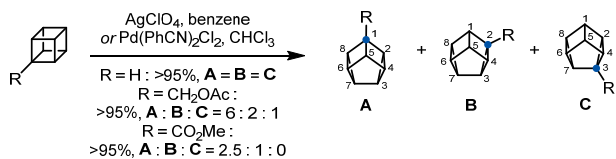
patterns to the reaction's progression "via the most economic bond-switching path." The relative amounts of 1,3- vs 2,6-isomer product formed was highly substituent-dependent. No significant advances in the synthesis of cuneanes were made for the following 50 years. However, during the preparation of this manuscript, Matsubara and coworkers reported the synthesis of enantioenriched, redundantly 2,6-substituted cuneanes using asymmetric silver and (preferentially) palladium catalysts.[8] The same manuscript describes the racemic, Ag[I]-catalyzed isomerization of 2 *asymmetrically* 1,4-disubstituted cubanes to 2,6-disubstituted cuneanes, the first such examples in the literature.

In the course of ongoing work involving the alkylation of cubane derivatives, we serendipitously observed the highly regioselective rearrangement of an *asymmetrically* 1,4-disubstituted cubane to one of the corresponding 1,3-cuneane isomers (Figure 1D). The value of this regioselectivity was immediately apparent as an entry point to a range of differentially 1,3-disubstituted cuneanes. We were surprised to find no literature precedent at the time for the rearrangement of such asymmetrically disubstituted substrates. We entered the study described herein to develop the scope of this transformation and determine key substituent effects on regioselectivity. Furthermore, we hoped to gain mechanistic understanding of the basis of the observed selectivity.
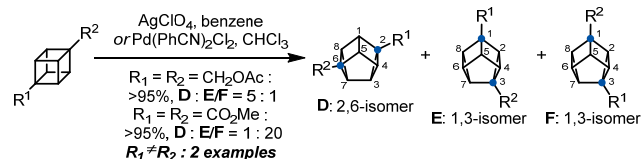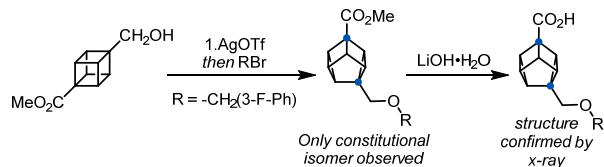
A. Cubane and cuneane: a comparison

cubane
>1000 SciFinder
substructure refs.[a]

• phenyl
bioisosterism

• energetic
materials

cuneane
<50 SciFinder
substructure refs.[a]

B. Eatons's original report: parent cubane and monosubstituted cubanes

AgClO$_4$, benzene
or Pd(PhCN)$_2$Cl$_2$, CHCl$_3$

R = H : >95%, **A = B = C**
R = CH$_2$OAc :
>95%, **A : B : C** = 6 : 2 : 1
R = CO$_2$Me :
>95%, **A : B : C** = 2.5 : 1 : 0

C. Eaton's original report: redundantly 1,4-disubstituted cubanes

AgClO$_4$, benzene
or Pd(PhCN)$_2$Cl$_2$, CHCl$_3$

R$_1$ = R$_2$ = CH$_2$OAc :
>95%, **D : E/F** = 5 : 1
R$_1$ = R$_2$ = CO$_2$Me :
>95%, **D : E/F** = 1 : 20
R$_1$≠R$_2$: 2 examples

D: 2,6-isomer   **E**: 1,3-isomer   **F**: 1,3-isomer

D. Our initial result: regioselective rearrangment/alkylation

1.AgOTf
then RBr

R = -CH$_2$(3-F-Ph)

LiOH•H$_2$O

*Only constitutional
isomer observed*

*structure
confirmed by
x-ray*

E. This work

AgTFA
toluene

2,6-isomer   1,3-isomers

Points of interest
• Interrogate
regioselectivity

• post-isomerization
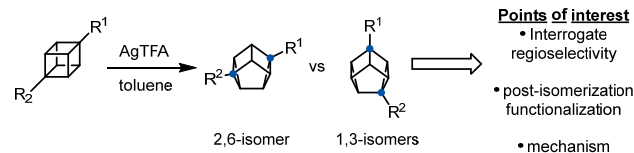functionalization

• mechanism

Figure 1.   Background on the limited chemistry of cuneanes.
[a] Reference counts made on the basis of SciFinder substructure searches conducted on 08/25/2022.

■ RESULTS AND DISCUSSION

We examined the isomerization of cubane **1a** as the model substrate using a variety of Ag^I catalysts in toluene at 80 °C (Table 1, entries 1-5). The regioselective isomerization occurred with 1 equivalent of AgTFA, providing desired cuneane in 70% yield (2,6- to 1,3-isomer ratio =13:1) (Table 1, entry 5). Many silver catalysts and the intermediates of ring strained isomerization are sensitive to heat and light. When this reaction was carried out without light, the yield was slightly increased with a 2,6- to 1,3-isomer ratio of 17:1 (Table 1, entry 6). The pure 2,6-cuneane compound could be isolated in 75% yield following recrystallization. Replacing AgTFA with Pd catalysts gave diminished yields, while replacing it with Lewis acids or TFA (trifluoroacetic acid) led to no product formation (Table 1, entries 7-9, see supporting information). The loading of catalyst and reaction temperature were then examined. When **1a** was reacted with a sub-stoichiometric amount of AgTFA or at 60 °C, cuneane was produced in 30% and 40% yields, respectively (Table 1, entries 10 and 11). Consistent with our original, serendipitous result, we found that **1f** isomerizes to give only a single 1,3-isomer, with no constitutional isomers detected. Furthermore, the best yield of **3f** (99%) was obtained under the reaction condition by using a sub-stoichiometric amount of Ag-TFA at 40 °C (Table 1, entry 13).
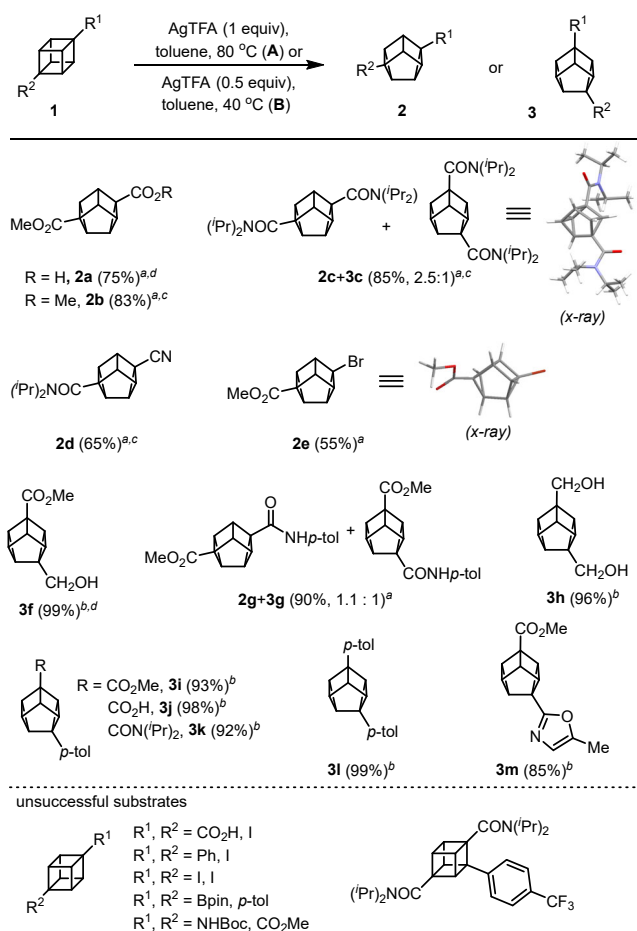
Table 1. Reaction optimization

entry	cat. (1 equiv)	R	temp (°C)	yield (2:3:3')(%)[a]
1	AgBF$_4$	CO$_2$H	80	5:0:0
2	AgPF$_6$	CO$_2$H	80	30:0:0
3	AgOAc	CO$_2$H	80	0:0:0
4	AgOTf	CO$_2$H	80	48:0:0
5	AgTFA	CO$_2$H	80	65:5 (3+3')
6[b]	**AgTFA**	**CO$_2$H**	**80**	**85:5 (3+3')** (75)[c,d]
7	PdCl$_2$	CO$_2$H	80	42:5 (3+3')
8	BF$_3$·Et$_2$O	CO$_2$H	80	0:0:0
9	TFA	CO$_2$H	80	0:0:0
10[b]	AgTFA (0.3)	CO$_2$H	80	30:0:0
11[b]	AgTFA	CO$_2$H	60	40:0:0
12[b]	AgTFA	CH$_2$OH	40	0:99:0
13[b]	**AgTFA (0.5)**	**CH$_2$OH**	**40**	**0:99:0**[d]

Reaction conditions: **1** (0.1 mmol, 1.0 equiv.) and catalyst (1.0 equiv.) were reacted in toluene (1.0 mL) for 15 h. [a]NMR yield using CH$_2$Br$_2$ as an internal standard. [b]Without light. [c]After recrystallization, only the isomer **2** was obtained. [d]Isolated yield.

Next, we explored the scope of the isomerization using 1,4-disubstituted cubanes under the optimized reaction conditions. Cubanes bearing two electron-withdrawing groups generally rearranged in high yields to the 2,6-isomer with modest to good selectivity. Reaction of 1-acid-4-methyl ester (**1a**), 1,4-dimethyl ester (**1b**), and 1-cyano-4-*N*,*N*-diisopropyl amide (**1d**) cubanes gave excellent selectivity for the 2,6-isomers **2a**, **2b**, and **2d,** respectively, in good yields. Furthermore, the potentially-sensitive bromide group of **2e** was also tolerated. However, 1,4-diamide (**1c**) and 1-amide-4-methylester (**1g**) cubanes underwent the rearrangement in good yield with poor regioselectivity. When cubanes bearing one electron-withdrawing and one electron-donating group were treated with AgTFA, single 1,3-isomers were produced in moderate to excellent yields. 1-methylester-4-hydroxymethyl (**1f**) and 1,4-dihydroxymethyl (**1h**) cubanes underwent rearrangement in 99% and 96% yields, respectively, providing 1,3-cuneanes **3f** and **3h**. Cubanes possessing one electron-withdrawing group and the *p*-tolyl moiety on the opposite vertex were gratifyingly compatible with the reaction conditions, generating **3i-3k** in 92-99% yields. Similarly, the rearrangement of a diaryl cubane (**1l**) took place efficiently in this reaction system to furnish **3l** in quantitative yield. A heteroaryl substituted cubane was easily converted to the corresponding cuneane **3m** obtained in 85% yield. Furthermore, this protocol was also compatible on a large scale; conducting the rearrangement with 5 mmol of **1a** and **1f** afforded the corresponding cuneanes **3a** and **3f** in 75% and 99% yields, respectively. Unfortunately, the rearrangement was unsuccessful with cubanes bearing -I, -Bpin, and -NHBoc groups, giving either almost no conversion or substrate decomposition to uncharacterized complex mixtures. Additionally, attempted rearrangement of a tri-substituted cubane under these reaction conditions resulted only in unproductive decomposition of the starting material.
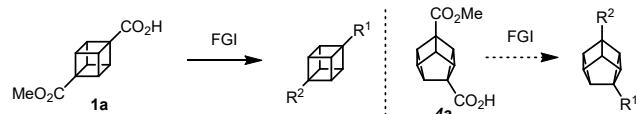
Table 2. Reaction Scope Study

R = H, **2a** (75%)[a,d]
R = Me, **2b** (83%)[a,c]

2c+3c (85%, 2.5:1)[a,c]

(x-ray)

2d (65%)[a,c]

2e (55%)[a]

(x-ray)

3f (99%)[b,d]

2g+3g (90%, 1.1 : 1)[a]

3h (96%)[b]

R = CO₂Me, **3i** (93%)[b]
CO₂H, **3j** (98%)[b]
CON(iPr)₂, **3k** (92%)[b]

3l (99%)[b]

3m (85%)[b]

unsuccessful substrates

R¹, R² = CO₂H, I
R¹, R² = Ph, I
R¹, R² = I, I
R¹, R² = Bpin, p-tol
R¹, R² = NHBoc, CO₂Me

[a]Condition A: **1** (0.1 mmol, 1.0 equiv.), AgTFA (1.0 equiv.), and toluene (0.1 M) were reacted at 80 °C in amber vial for 15 h. Isolated yield. [b]Condition B: **1** (0.1 mmol, 1.0 equiv.), AgTFA (0.5 equiv.), and toluene (0.1 M) were reacted at 40 °C in amber vial for 15 h. [c]Reaction for 30 h. [d]5 mmol scale.

To establish the synthetic value of functionalized cuneanes accessible via Ag-catalyzed rearrangement, we explored a variety of subsequent functional group manipulations. Compound **4a** emerged as a potentially useful synthetic intermediate to target in our study. "Half-esters" of alkyl diacids serve as common, useful building blocks for the preparation of differentially disubstituted sp³-rich scaffolds.[10] Indeed, commercially available cubane **1a** served as a convenient starting material for our substrate scope study. While **2a** could serve as a general precursor to 2,6-disubstituted cuneanes, previously unknown compound **4a** could serve the same role for 1,3-disubstituted cuneanes. Several possible routes to **4a** were considered (Figure 2B). Compared to the alternative black and red routes, the route shown in blue is highly efficient; the regioselective rearrangement of **1f** to **3f** more than compensates for its requisite oxidation state manipulations.

A. Half-ester of 1,3-cuneane diacid as a useful building block
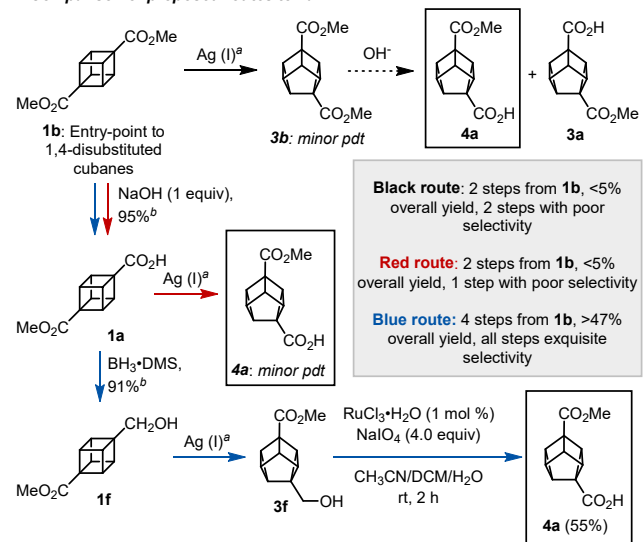

B. Comparison of proposed routes to 4a

Black route: 2 steps from **1b**, <5% overall yield, 2 steps with poor selectivity

Red route: 2 steps from **1b**, <5% overall yield, 1 step with poor selectivity

Blue route: 4 steps from **1b**, >47% overall yield, all steps exquisite selectivity

Figure 2. Building blocks accessed via oxidation and reduction. [a]See Table 2 for yield and selectivity data [b]Previously reported[9]; FGI = functional group interconversions

Given the value of amines as building blocks for medicinal chemistry and the apparent incompatibility of carbamates with the reaction conditions, we aimed to install nitrogenous functionality on a pre-formed cuneane. Curtius rearrangement of **2a** provided isolable carbamate **4c** in high yield (Figure 3, eq 1). Exposure of **4c** to acids failed to yield amine hydrochloride **5b**, but instead afforded ketone **5a** in 90% yield (Figure 3, eq 2), the structure of which was determined via single-crystal X-ray diffraction analysis of its dinitrophenylhydrazone (Figure 3, eq 3). Similar ketone-forming reactivity is precedented with other strained-ring amines such as bicyclo[2.2.0]hexan-1-amine.[11] Cubylamines are also prone to ring-opening, though their hydrochloride salts are generally isolable.[3]

Further experiments were conducted to compare the reactivity of cubane and cuneane congeners. For instance, we were able to repeat Itami's recent work demonstrating the *ortho*-lithiation/zincate formation and Negishi coupling of cubanes.[12] However, subjecting **2d** to the same conditions showed no desired reactivity and decomposition of the starting material (Figure 4, eq 1). Gratifyingly, decarboxylative arylation of **2o** gave 54% yield of **2p** under nickel catalysis with an electron-poor, substituted bipyridine ligand system (Figure 4, eq 2).[13] Cuneane **2p** is notably inaccessible via direct rearrangement of the corresponding cubane **1i**, which exclusively gives the 1,3-disubstituted cuneane **3i** upon exposure to AgTFA (vide supra).
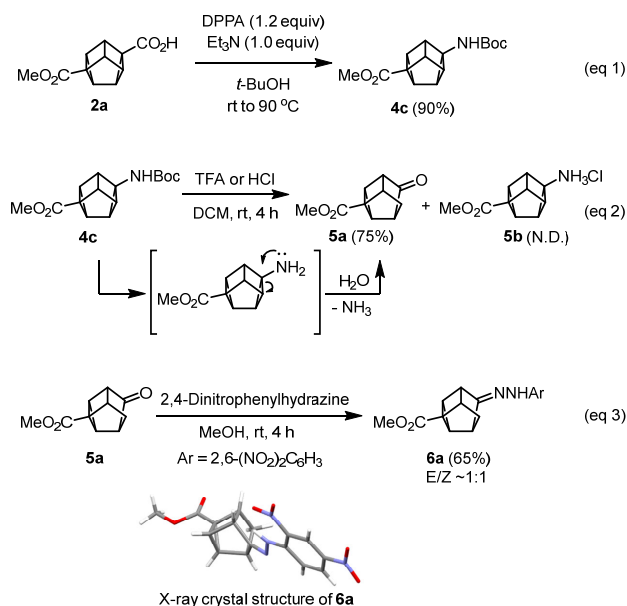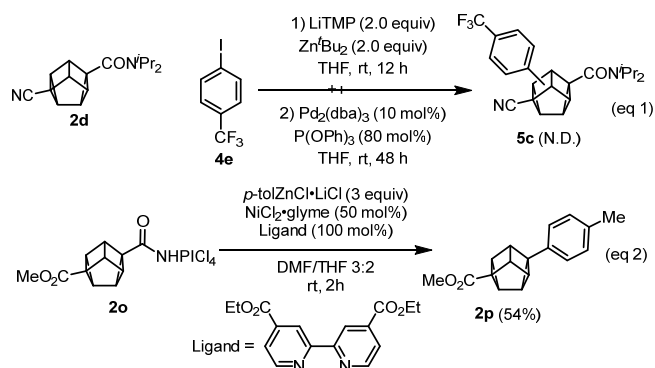
Figure 3. Curtius rearrangement and hydrolysis

Figure 4. Arylation of cuneane skeleton; NHPICl$_4$ = tetrachlorophthalimide N-oxyl group

We next sought to compare the energetic behavior of nitrated cubane and cuneane derivatives, specifically the nitrate esters **5d**, **5e**, and **5f** (Figure 5). The 2,6-cuneane **2h**, inaccessible by direct isomerization, was prepared by reduction of **2a** and was obtained in 75 % yield (Figure 5, eq. 1). Frustratingly, attempts at nitration of **2h** and **3h** using the relatively mild nitrating agent acetyl nitrate led only to unproductive decomposition to complex mixtures, which presented as low-energy gums, suggesting inadvertent destruction of the cuneane skeleton (Figure 5, eq. 2-3). However, cubane **1h** was successfully nitrated using acetyl nitrate to give previously reported nitrate ester **5f** (Figure 5, eq. 4).[14-18] The isolation process required modification to provide sufficiently pure material for analysis. We found that trituration of the gummy, impure concentrate of the dichloromethane extract using ethyl acetate gave pure **5f** as a white, crystalline solid. While this nitration procedure and isolation proved robust and scalable, attempted nitration of **1h** with chilled nitric acid led to spontaneous ignition (hypergolic behavior).
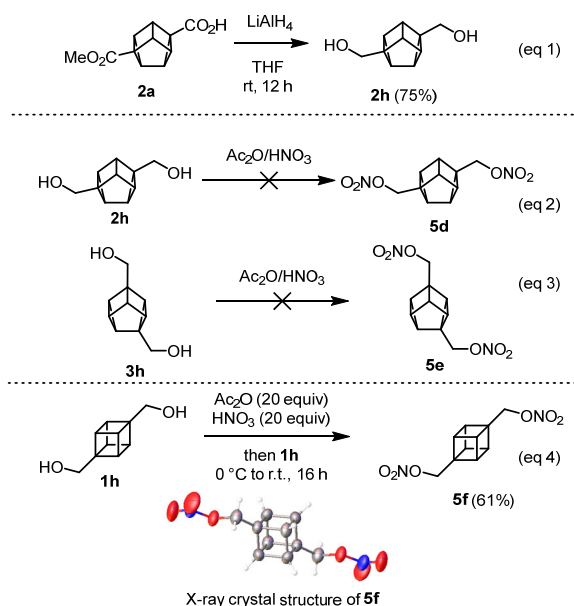

Figure 5. Efforts towards cubane and cuneane nitrate esters

The energetic properties of **5f** were determined through a combination of experimental and computational techniques (Table 3). Differential scanning calorimetry showed a sharp, exothermic decomposition of **5f** beginning at 141 °C, somewhat higher than the reported decomposition temperature of 123-124 °C.[15] No melting was observed prior to decomposition. Impact and friction sensitivities were determined according to the NATO STANAG guidelines.[19-20] The density of 1.516 g/cm^3, determined using single crystal X-ray diffraction crystallography, is comparable to the previously reported value of 1.512 g/cm^{-3}.[15]

Table 3: Physical and energetic properties of dinitratomethyl cubane 5f.

Data category	Dinitratomethyl cubane
T_{dec} [^{o}C][a]	141.0
Ω_{CO2} [%][b]	-119.7
Ω_{CO} [%][c]	-56.7
ρ [gcm^{-3}][d]	1.516
P_{cj} [GPa][e]	17.2
V_{det} [ms^{-1}][f]	7116
I_{sp} [s][g]	224.8
$\Delta_f H°$ [kJ mol^{-1}][h]	244.9
IS[i] [J]	7.0
FS[j] [N]	156
ESD[k] [J]	0.125

Computations were performed to study the isomerization reaction mechanism and origins of regioselectivity, combining static and dynamic trajectory calculations. Density functional theory (DFT) calculations were carried out with TURBOMOLE 7.3[21] and ORCA 4.2.1.[22] Conformer sampling was done using xTB,[23] CREST,[24] and CENSO[25] program packages. Geometry optimizations and vibrational frequencies were calculated using the dispersion corrected hybrid functional PBE0-D3(0)[26, 27] with the def2-TZVP[28] basis set since PBE0 gives good geometries for transition metal complexes.[29-31] Final gas-phase single-point energy calculations were carried out with random phase approximation (RPA)[32] using PBE0/def2-QZVPP orbitals. Solvation effects for toluene were accounted for using COSMO[33-35] for geometries and frequencies and COSMO-RS[33, 36-38] for single-point energies. Additionally, we used Grimme's quasi-RRHO approximation.[39] Gas-phase Born-Oppenheimer molecular dynamics (BOMD) trajectory calculations were initialized and propagated in Gaussian 16[40] with energies and gradients evaluated at the PBE0-D3/def2-TZVP level of theory. Full computational details are presented in the SI.

In experiment, substrate-dependent selectivity for either 1,3 or 2,6-cuneanes was observed. To rationalize these observations, we first studied the isomerization mechanism of **1b** since it gave 2,6-cuneane **2b** as the major product and 1,3-cuneane **3b** as a minor product. While the kinetics of related isomerization reactions have been studied,[41-42] to the best of our knowledge, computational mechanistic studies of the cubane to cuneane isomerization have not been previously reported. Our calculations reveal a reactive potential energy surface (PES) that is highly complex: distinct mechanistic pathways converge to form the same regioisomeric product, the identity of the rate-limiting TS varies across pathways, and the presence of non-classical carbocationic intermediates. Further, we employed non-statistical dynamic calculations to study selectivity of branching points that were skipped on the static PES.

A recent review concluded that the reactive silver(I) salt can be either mononuclear or binuclear, although the distinction is difficult to make.[44] We considered the reactive Ag(I) species as mononuclear. Accounting for the homolytic dissociation of the Ag(I) dimer is challenging and will affect the absolute free energies for the whole PES. However, using **Int-1** as the reference state for both mononuclear and binuclear mechanisms, i.e., circumventing the effect of the dimer dissociation, lead to lower barriers for the mononuclear mechanism with **1b**. Furthermore,

we could formulate the same conclusions from both mechanisms except for the identity of the major pathway, see SI. The isomerization of **1b** is initiated by Ag(I) insertion to one of the cubane's two inequivalent C–C bonds; C1–C2 (**TS1$_{C1-C2}$**) or C2–C2 (**TS1$_{C2-C2}$**) (Figure 6a). This is the first branching point in the mechanism: C2–C2 insertion ultimately leads toward a single product (**2b**), whereas the regiochemical outcome (**2b** vs **3b**) of C1–C2 insertion is decided at the next step.

Addition to the C2–C2 bond had an activation free energy barrier of 26.8 kcal·mol^{-1} and was favored over C1–C2 addition by 3.2 kcal·mol^{-1}. In the bridged C2-Ag-C2 intermediate (**Int-2$_{C2-C2}$**) formed in this first step, one of the equivalent Ag–C2 bonds can break heterolytically. This kinetic barrier constitutes the turnover determining step for the major (C2–C2, **2b**) pathway at 28.2 kcal·mol^{-1} (**TS2$_{C2Ag-C2}$**). The pathway selectively formed the experimentally observed major product **2b** and no subsequent intermediates or branching points were located, confirmed by dynamic reaction coordinate calculations showing the evolution of **TS2** to cuneane product **2b**. Interestingly, with substrate **1i**, see below, a nonclassical carbocationic intermediate is found on the PES following Ag–C cleavage. From the C1-Ag-C2 intermediate, two possible cleavage pathways can take place: breaking of the Ag–C1 bond yields the minor product regioisomer **3b** ($\Delta G^{\ddagger}$ = 31.2 kcal·mol^{-1}), whereas breaking the Ag–C2 bond yields the major product, **2b** ($\Delta G^{\ddagger}$ = 26.8 kcal·mol^{-1}). The mechanism for substrate **1b** isomerization thus revealed that two pathways contribute to the major product formation; major(C2–C2, **2b**) and minor(C1–C2, **2b**) with 88.0% and 11.9% contributions, respectively, while each of the three branches had different turnover determining steps.

To understand the regioselectivity, we analyzed NBO charges along the major(C2-C2, **2b**) reaction coordinate (Figure 6b). Compared to the substrate·AgTFA complex **Int-1**, in both **TS1$_{C2-C2}$** and **Int-2$_{C2-C2}$**, the two carbons now attached to silver gain electron density (ΔNBO < 0), while the catalyst loses electron density. This net transfer of charge from catalyst to substrate is indicative of C-C oxidative insertion, which accounts for the lower barrier of insertion into the C2–C2 bond. Accordingly, we expect the initial insertion will generally favor more electron-rich $_{C-C}$ bonds of cubane derivatives: in this case, the C1–C2 bond is less electron-rich (α-position of the methyl ester), and **TS1$_{C1-C2}$** has a higher activation free energy barrier by more than 3 kcal·mol^{-1}. In the next step, i.e., **TS2$_{C2Ag-C2}$** in Figure 6b, Ag–C bond-breaking is accompanied by substantial charge separation involving the accumulation of carbocationic character at the separating carbon atom. Due to symmetry in **Int-2$_{C2-C2}$**, fragmentation of either Ag-C bond is degenerate. However, for the minor pathway, cleavage of the Ag–C2 bond is favored over Ag–C1 by more than 4 kcal·mol^{-1} since the build-up of positive charge at C1 is substantially less favorable (see Figure 6a).

We next investigated the isomerization of substrates **1i** and **1f**, which result in opposite regioselectivity to **1b**, selectively forming the 1,3-cuneane product. Oxidative addition barriers for these less electron-deficient substrates are several kcal·mol^{-1} lower than for **1b**, with insertion preferentially occurring away from the electron-

a) Reaction free energy profile for **1b**
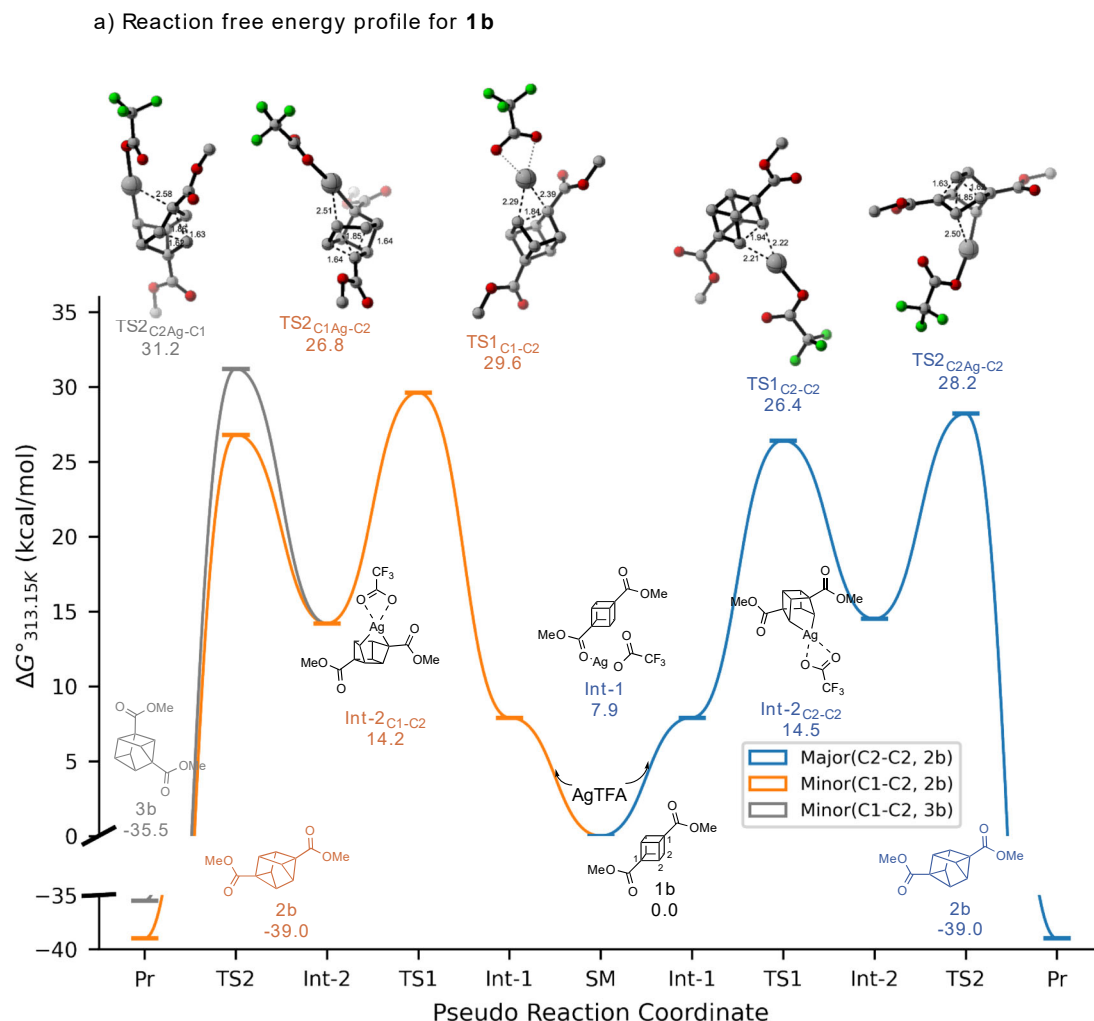
b) ΔNBO charges along Major(C2-C2, **2b**)
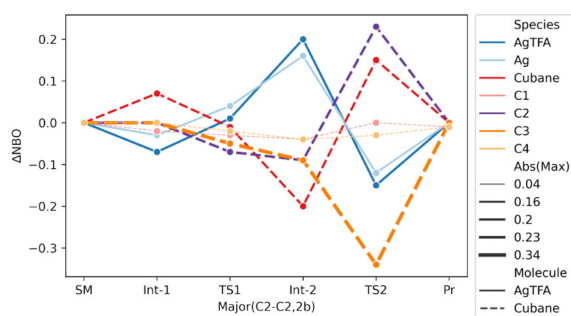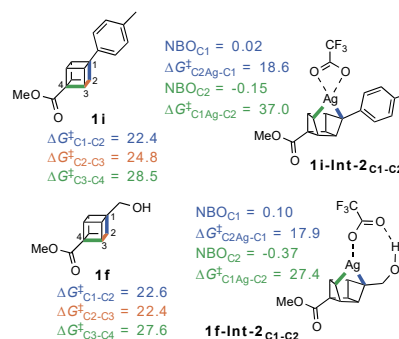
c) Regioselectivity for **1f** and **1i**

Figure 6. a) Reaction free energy profile for isomerization of **1b** to **2b** and **3b** in kcal·mol⁻¹ at 353.15 K; b) ΔNBO graph for C1–4 and Ag atoms, as well as **1b** and AgTFA moieties for major(C2–C2, **2b**) pathway; and c) activation free energy barriers at 313.15 K for regioselectivity determining steps for **1f** and **1i** with NBO charges in **Int-2$_{C1-C2}$**. The free energies were computed at RPA@PBE0-D3/def2-QZVPP//PBE0-D3/def2-TZVP in toluene (COSMO-RS//COSMO) level of theory. See SI for full computational details.

withdrawing ester group. For **1i**, addition adjacent to the aromatic ring at the C1–C2 bond is favored over the C2–C3 or C3–C4 bonds with activation free energy barriers of 22.4, 24.8, and 28.5 kcal·mol⁻¹, respectively (Figure 6c). Subsequent breaking of the Ag–C1 bond is then favored over the Ag–C2 bond (Figure 6c), with positive charge accumulating at the benzylic position in **TS2$_{C2Ag-C1}$**. The ensuing intermediate is a nonclassical

carbocation,[44] which falls to the final 1,3-cuneane product, **3i**, with a very small barrier of 0.2 kcal·mol⁻¹.

For **1f**, C1–C2 and C2–C3 additions are nearly isoenergetic with activation free energy barriers of 22.6 and 22.4 kcal·mol⁻¹, respectively, whereas C3–C4 addition is significantly higher at 27.6 kcal·mol⁻¹ (see Figure 6c). In both
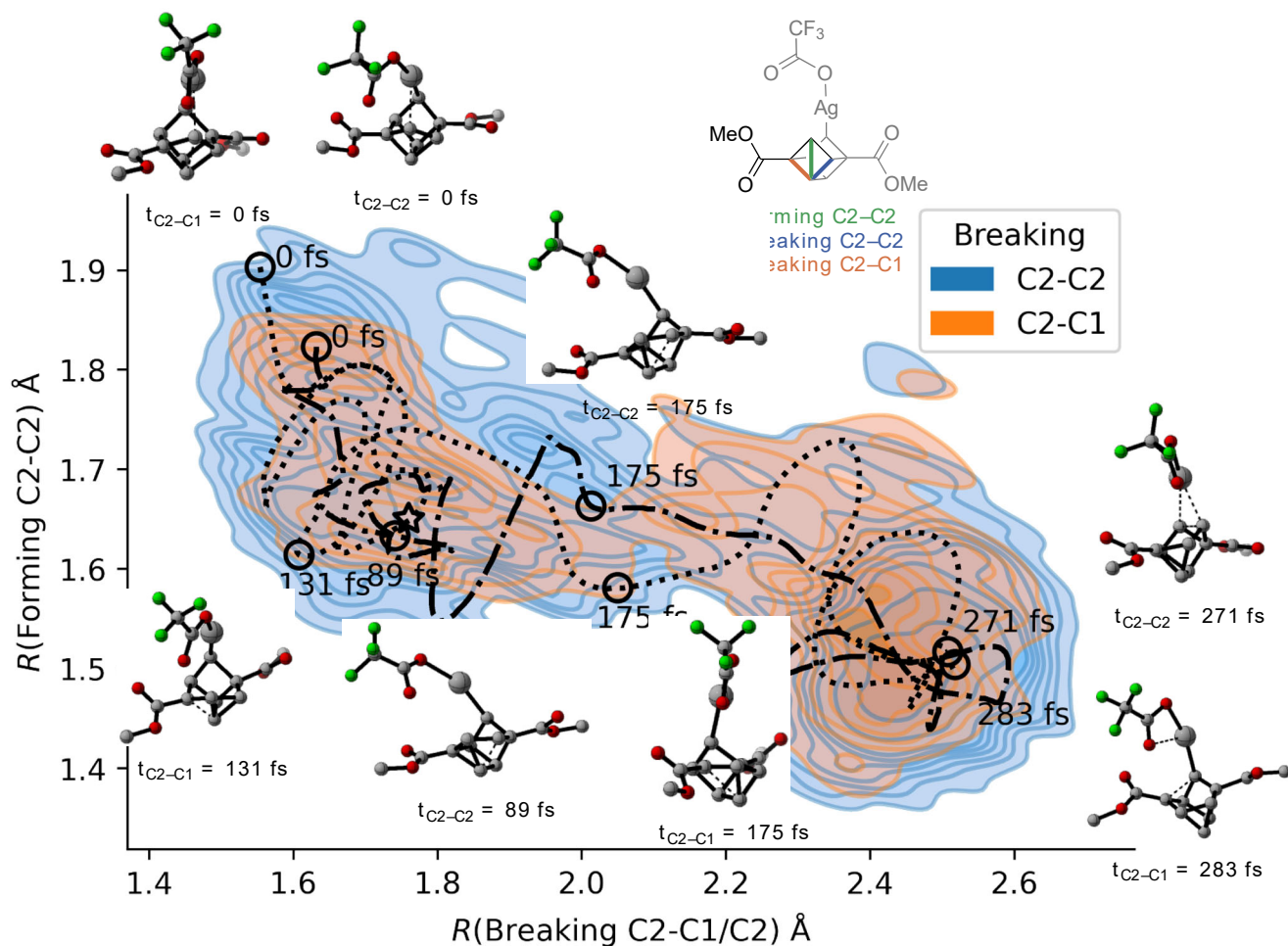
Figure 7. Plot of two representative trajectories for substrate **1b** starting at **TS2$_{C2Ag-C2}$** (0 femtoseconds (fs)) plotted as forming C2-C2 bond length (y-axis) against breaking C2-C1 or C2-C2 bond length (x-axis). The blue and orange contour plots sum the 19 forward trajectories: blue for forming product **2b** (breaking C2-C2 bond) and orange for forming product **3b** (breaking C2-C1). The dashed-dotted line is a trajectory that ends at **2b** (blue area) and the dotted line is a trajectory that ends at **3b** (orange area). The star indicates the position of DFT optimized nonclassical carbocation (SI) and circles pinpoint time of structure snapshot displayed in 3D. For full details, see SI.

TS1$_{C1-C2}$ and **TS1$_{C2-C3}$**, the hydroxyl group of **1f** is hydrogen-bonded to the TFA oxygen, but only the C2–C3 activation free energy barrier was lowered compared to **1i**. The charge separation was even more pronounced in **1f-Int-2$_{C1-C2}$** than in **1i-Int-2$_{C1-C2}$** and, again, the Ag–C bond to more electropositive carbon was broken leading to the major product **3f**. Likewise, the two carbons in **1f-Int-2$_{C2-C3}$** demonstrated divergent polarization – C2 becoming more positive and C3 more negative – and the scission of the Ag–C2 bond was favored (see SI). Since the turnover determining step for both C1–C2 and C2–C3 bond activation were isoenergetic with **1f**, both pathways contribute almost equally to the formation of **3f**. Again, while the Ag-C bond scission in **TS2$_{C2Ag-C1}$** can only evolve to **3f**, **TS2$_{C3Ag-C2}$** (SI) on the other hand could potentially lead to both **2f** and **3f**, while dynamic reaction coordinate calculation connected **TS2$_{C3Ag-C2}$** to only **3f**.

Because the static potential-energy surface indicated intermediates with significant carbocation character, nonclassical bonding (**1i-Int-3**, see SI), and possible bifurcation points (e.g. after **TS2$_{C2Ag-C2}$**) that could lead to both major and minor products, we initiated quasiclassical direct dynamics trajectory calculations. Trajectories initiated from transition-state structures

were sampled using zero-point and thermal local mode sampling at 343 K and propagated with an average time step of 0.5 fs. Figure 7 plots two representative trajectories started at **TS2$_{C2Ag-C2}$** (for **1b**). One trajectory leads to **2b** and the other **3b**. In both trajectories a non-classical carbocation type structure occurs close to 100 fs after the transition state, but this structure is extremely short-lived and within another 100 fs evolves to become either **2b** or **3b**, which indicates this intermediate might be best considered dynamically skipped. From 20 trajectories, only one trajectory recrossed to **Int-2$_{C2-C2}$**, 15 ended at the major product **2b**, and four ended at the minor product **3b**. This indicates that in addition to transition state selectivity there is also dynamic selectivity, however, the transition state predicts the major product.

Thus, based on careful computational analysis, a set of qualitative rules could be established for the activation of 1,4-substituted cubanes. First, the initial addition favors more electron-rich C–C σ-bonds, such as those adjacent to an electron-donating group, *e.g.*, C1–C2 with substrates **1f** and **1i**, or remote from electron-withdrawing groups, like C2–C2 for **1b**. Second, the two carbons attached to silver in bridging **Int-2** exhibit charge separation if the carbons are not equivalent. Ag-C cleavage

results in an accumulation of carbocationic character more favorably adjacent to an electron-donating substituent and is avoided adjacent to an electron-withdrawing group, as in **TS2$_{C1Ag-C2}$** and **TS2$_{C2Ag-C1}$**. Third, at least two distinct pathways converge to form the major regioisomer. In our static studies of the PES for **1i**, a metastable nonclassical carbocation intermediate is formed by Ag-C bond breaking, with a small barrier towards cuneane formation. For **1b**, such an intermediate is skipped on the PES. However, quasiclassical dynamic trajectories indicate that a similar nonclassical carbocation occurs as a transient, dynamic intermediate, serving as a bifurcation point for products **2b** and **3b**. Thus, while transition states provide prediction of the major product the regioselectivity is partially influenced by dynamic effects.

◼CONCLUSIONS

In summary, we have further developed the Ag^I-catalyzed isomerization of cubanes to cuneanes with an emphasis on the generation on differentially 1,3-disubstituted cuneanes. We explored the convoluted mechanism of the reaction computationally and were able to develop a predictive model for the observed regioselectivity trends. We achieved several functional group interconversions on the cuneane scaffold, but its skeleton appears to make derivatives more fragile than the corresponding cubanes, despite having lower strain energy. This relative kinetic sensitivity (to a variety of conditions) may be a consequence of cuneane's embedded cyclopropane rings. Skeletal sensitivity hindered our study of energetic nitrate ester derivatives but led us to extensively characterize the analogous cubane **5f**. Despite the imperfect translation of cubane reactivity onto cuneane congeners, we hope this work will facilitate the study of cuneane derivatives, particularly differentially disubstituted species, in diverse applications.

ASSOCIATED CONTENT

Supporting Information.
Experimental procedures, characterization data, NMR spectra, and X-ray crystallographic data

Accession Codes

CCDC 2114060, 2123861, 2113847, 2123862, 2113848, and 2215914, contain the supplementary crystallographic data for this paper. These data can be obtained free of charge via www.ccdc.cam.ac.uk/data_request/cif, or by emailing data_request@ccdc.cam.ac.uk, or by contacting The Cambridge Crystallographic Data Centre, 12 Union Road, Cambridge CB2 1EZ, UK; fax: +44 1223 336033.

AUTHOR INFORMATION

Corresponding Authors

*Daniel H. Ess − Department of Chemistry and Biochemistry, Brigham Young University, Provo, Utah 84602, United States; orcid.org/0000-0001-5689-9762; Email: dhe@ chem.byu.edu

*Robert S. Paton − Department of Chemistry, Colorado State University, Fort Collins, Colorado 80523, United States; orcid.org/0000-0002-0104-4166; Email: robert.paton@ colostate.edu

*Corey R. J. Stephenson − Department of Chemistry, Willard Henry Dow Laboratory, University of Michigan, Ann Arbor, Michigan 48109, United States; orcid.org/0000-0002-2443-5514; Email: crjsteph@umich.edu

Author Contributions

‡These authors contributed equally.

Notes
The authors declare no competing financial interest.

ABBREVIATIONS

AgTFA, silver (I) trifluoroacetate; FGI, functional group interconversion, NHPICl$_4$, tetrachlorophthalimide N-oxyl

REFERENCES

1. Eaton, P. E.; Cole, T. W., The Cubane System. *Journal of the American Chemical Society* **1964,** *86* (5), 962-964.
2. Eaton, P. E., Zhang, Mao-Xi, Octanitrocubane: A New Nitrocarbon. *Propellants, Explosive, Pyrotechnics* **2002,** *27*, 1-6.
3. Eaton, P. E., Cubanes: Starting Materials for the Chemistry of the 1990s and the New Century. *Angewandte Chemie International Edition in English* **1992,** *31* (11), 1421-1436.
4. Chalmers, B. A.; Xing, H.; Houston, S.; Clark, C.; Ghassabian, S.; Kuo, A.; Cao, B.; Reitsma, A.; Murray, C. E. P.; Stok, J. E.; Boyle, G. M.; Pierce, C. J.; Littler, S. W.; Winkler, D. A.; Bernhardt, P. V.; Pasay, C.; De Voss, J. J.; McCarthy, J.; Parsons, P. G.; Walter, G. H.; Smith, M. T.; Cooper, H. M.; Nilsson, S. K.; Tsanaktsidis, J.; Savage, G. P.; Williams, C. M., Validating Eaton's Hypothesis: Cubane as a Benzene Bioisostere. *Angewandte Chemie International Edition* **2016,** *55* (11), 3580-3585.
5. Al-Janabi, A.; Mandle, R. J., Utilising Saturated Hydrocarbon Isosteres of para Benzene in the Design of Twist-Bend Nematic Liquid Crystals. *ChemPhysChem* **2020,** *21* (8), 697-701.
6. Bényei, G.; Jalsovszky, I.; Demus, D.; Prasad, K.; Rao, S.; Vajda, A.; Jákli, A.; Fodor-Csorba, K., First liquid crystalline cuneane-caged derivatives: a structure–property relationship study. *Liq. Cryst.* **2006,** *33* (6), 689-696.
7. Eaton, P. E.; Cassar, L.; Halpern, J., Silver(I)- and palladium(II)-catalyzed isomerizations of cubane. Synthesis and characterization of cuneane. *J. Am. Chem. Soc.* **1970,** *92* (21), 6366-6368.
8. Takebe, H.; Matsubara, S. Catalytic Asymmetric Synthesis of 2,6-Disubstituted Cuneanes through Enantioselective Constitutional Isomerization of 1,4-Disubstituted Cubanes *Eur. J. Org. Chem.* **2022,** e202200567
9. Houston, S. D.; Xing, H.; Bernhardt, P. V.; Vanden Berg, T. J.; Tsanaktsidis, J.; Savage, G. P.; Williams, C. M., Cyclooctatetraenes through Valence Isomerization of Cubanes: Scope and Limitations. *Chemistry – A European Journal* **2019,** *25* (11), 2735-2739.
10. Mykhailiuk, P. K., Saturated bioisosteres of benzene: where to go next? *Organic & Biomolecular Chemistry* **2019,** *17* (11), 2839-2849.

11.   Kirmse, W.; Sandkühler, P., Synthese und Umlagerung 1-substituierter Bicyclo[2.2.0]hexane. *Liebigs Annalen der Chemie* **1981,** *1981* (8), 1394-1406.

12.   Okude, R.; Mori, G.; Yagi, A.; Itami, K., Programmable synthesis of multiply arylated cubanes through C–H metalation and arylation. *Chemical Science* **2020,** *11* (29), 7672-7675.

13.   Qin, T.; Malins, L. R.; Edwards, J. T.; Merchant, R. R.; Novak, A. J. E.; Zhong, J. Z.; Mills, R. B.; Yan, M.; Yuan, C.; Eastgate, M. D.; Baran, P. S., Nickel-Catalyzed Barton Decarboxylation and Giese Reactions: A Practical Take on Classic Transforms. *Angewandte Chemie International Edition* **2017,** *56* (1), 260-265.

14.   Dubikin, V. V.; Prokudin, V. G.; Nazina, L. D.; Romanova, L. B.; Eremenko, L. T.; Nazin, G. M. Kinetics and mechanism of the thermal decomposition of 1-bromo-4-nitroxymethylcubane. *Kinetics and Catalysis* **2007,** *48*, 345-347.

15.   Romanova, L. B.; Barinova, L. S.; Zakharov, V. V.; Eremenko, L. T.; Aleksandrov, G. G.; Eremenko, I. L. Cubane derivatives 10. Synthesis and molecular structures of nitroxymethylcubanes. *Russian Chemical Bulletin* **2010,** *59*, 1051-1055.

16.   Nesterenko, D. A.; Garanin, V. A.; Kazakov, A. I.; Korepin, A. G.; Romanova, L. B. Energetic properties and impact sensitivity of crystalline explosives. *Russian Journal of Physical Chemistry B* **2014,** *8*, 701-711.

17.   Lempert, D. B.; Zyuzin, I. N.; Averkov, I. S.; Raznoschikov, V. V.; Yanovskii, L. S. Some Cubane Derivatives as Potential Components of Solid Gas Generator Propellants. *Russian Journal of Applied Chemistry* **2021,** *94*, 172-181.

18.   Lal, S.; Bhattacharjee, A.; Chowdhury, A.; Kumbhakarna, N.; Namboothiri, I. N. N. Approaches to 1,4-Disubstituted Cubane Derivatives as Energetic Materials: Design, Theoretical Studies and Synthesis. *Chem. Asian J.* **2022,** *17*, e2022004.

19.   *NATO Standardization Agreement (STANAG) on Explosives, Friction Sensitivity Tests, No. 4487, 1st ed.,* August 22, **2002**.

20.   *NATO Standardization Agreement (STANAG) on Explosives, Impact Sensitivity Tests, No. 4489, 1st ed.,* September 17, **1999**.

21.   Balasubramani, S. G.; Chen, G. P.; Coriani, S.; Diedenhofen, M.; Frank, M. S.; Franzke, Y. J.; Furche, F.; Grotjahn, R.; Harding, M. E.; Hättig, C.; Hellweg, A.; Helmich-Paris, B.; Holzer, C.; Huniar, U.; Kaupp, M.; Khah, A. M.; Khani, S. K.; Müller, T.; Mack, F.; Nguyen, B. D.; Parker, S. M.; Perlt, E.; Rappoport, D.; Reiter, K.; Roy, S.; Rückert, M.; Schmitz, A.; Sierka, M.; Tapavicza, E.; Tew, D. P.; Wüllen, C. v.; Voora, V. K.; Weigend, F.; Wodyński, A.; Yu, J. M., TURBOMOLE: Modular program suite for ab initio quantum-chemical and condensed-matter simulations. *J. Chem. Phys.* **2020,** *152* (18), 184107.

22.   Neese, F., Software update: the ORCA program system, version 4.0. *WIREs Comput. Mol. Sci.* **2018,** *8* (1), e1327.

23.   Grimme, S.; Bannwarth, C.; Shushkov, P., A Robust and Accurate Tight-Binding Quantum Chemical Method for Structures, Vibrational Frequencies, and Noncovalent Interactions of Large Molecular Systems Parametrized for All spd-Block Elements (Z = 1–86). *J. Chem. Theory Comput.* **2017,** *13* (5), 1989-2009.

24.   Pracht, P.; Bohle, F.; Grimme, S., Automated exploration of the low-energy chemical space with fast quantum chemical methods. *Phys. Chem. Chem. Phys.* **2020,** *22* (14), 7169-7192.

25.   Grimme, S.; Bohle, F.; Hansen, A.; Pracht, P.; Spicher, S.; Stahn, M., Efficient Quantum Chemical Calculation of Structure Ensembles and Free Energies for Nonrigid Molecules. *J. Phys. Chem. A* **2021,** *125* (19), 4039-4054.

26.   Adamo, C.; Barone, V., Toward reliable density functional methods without adjustable parameters: The PBE0 model. *J. Chem. Phys.* **1999,** *110* (13), 6158-6170.

27.   Grimme, S.; Antony, J.; Ehrlich, S.; Krieg, H., A consistent and accurate ab initio parametrization of density functional dispersion correction (DFT-D) for the 94 elements H-Pu. *J. Chem. Phys.* **2010,** *132* (15), 154104.

28.   Weigend, F.; Ahlrichs, R., Balanced basis sets of split valence, triple zeta valence and quadruple zeta valence quality for H to Rn: Design and assessment of accuracy. *Phys. Chem. Chem. Phys.* **2005,** *7* (18), 3297-3305.

29.   Bühl, M.; Reimann, C.; Pantazis, D. A.; Bredow, T.; Neese, F., Geometries of Third-Row Transition-Metal Complexes from Density-Functional Theory. *J. Chem. Theory Comput.* **2008,** *4* (9), 1449-1459.

30.   Waller, M. P.; Braun, H.; Hojdis, N.; Bühl, M., Geometries of Second-Row Transition-Metal Complexes from Density-Functional Theory. *J. Chem. Theory Comput.* **2007,** *3* (6), 2234-2242.

31.   Cramer, C. J.; Truhlar, D. G., Density functional theory for transition metals and transition metal chemistry. *Phys. Chem. Chem. Phys.* **2009,** *11* (46), 10757-10816.

32.   Chen, G. P.; Voora, V. K.; Agee, M. M.; Balasubramani, S. G.; Furche, F., Random-Phase Approximation Methods. *Annu. Rev. Phys. Chem.* **2017,** *68* (1), 421-445.

33.   Klamt, A., The COSMO and COSMO-RS solvation models. *WIREs Comput. Mol. Sci.* **2018,** *8* (1), e1338.

34.   Schäfer, A.; Klamt, A.; Sattel, D.; Lohrenz, J. C. W.; Eckert, F., COSMO Implementation in TURBOMOLE: Extension of an efficient quantum chemical code towards liquid systems. *Phys. Chem. Chem. Phys.* **2000,** *2* (10), 2187-2193.

35.   Klamt, A.; Schüürmann, G., COSMO: a new approach to dielectric screening in solvents with explicit expressions for the screening energy and its gradient. *Journal of the Chemical Society, Perkin Transactions 2* **1993,** (5), 799-805.

36.   Klamt, A. *COSMOtherm*, 19; COSMOlogic GmbH & Co. KG, a Dassault Systèmes company.: 2019.

37.   Klamt, A.; Jonas, V.; Bürger, T.; Lohrenz, J. C. W., Refinement and Parametrization of COSMO-RS. *J. Phys. Chem. A* **1998,** *102* (26), 5074-5085.

38.   Klamt, A., Conductor-like Screening Model for Real Solvents: A New Approach to the Quantitative Calculation of Solvation Phenomena. *J. Phys. Chem.* **1995,** *99* (7), 2224-2235.

39.   Grimme, S., Supramolecular Binding Thermodynamics by Dispersion-Corrected Density Functional Theory. *Chem. Eur. J.* **2012,** *18* (32), 9955-9964.

40.   Frisch, M. J.; Trucks, G. W.; Schlegel, H. B.; Scuseria, G. E.; Robb, M. A.; Cheeseman, J. R.; Scalmani, G.; Barone, V.; Petersson, G. A.; Nakatsuji, H.; Li, X.; Caricato, M.; Marenich, A. V.; Bloino, J.; Janesko, B. G.; Gomperts, R.; Mennucci, B.; Hratchian, H. P.; Ortiz, J. V.; Izmaylov, A. F.; Sonnenberg, J. L.; Williams; Ding, F.; Lipparini, F.; Egidi, F.; Goings, J.; Peng, B.; Petrone, A.; Henderson, T.; Ranasinghe, D.; Zakrzewski, V. G.; Gao, J.; Rega, N.; Zheng, G.; Liang, W.; Hada, M.; Ehara, M.; Toyota, K.; Fukuda, R.; Hasegawa, J.; Ishida, M.; Nakajima, T.; Honda, Y.; Kitao, O.; Nakai, H.; Vreven, T.; Throssell, K.; Montgomery Jr., J. A.; Peralta, J. E.; Ogliaro, F.; Bearpark, M. J.; Heyd, J. J.; Brothers, E. N.; Kudin, K. N.; Staroverov, V. N.; Keith, T. A.; Kobayashi, R.; Normand, J.; Raghavachari, K.; Rendell, A. P.; Burant, J. C.; Iyengar, S. S.; Tomasi, J.; Cossi, M.; Millam, J. M.; Klene, M.; Adamo, C.; Cammi, R.; Ochterski, J. W.; Martin, R. L.; Morokuma, K.; Farkas, O.; Foresman, J. B.; Fox, D. J. *Gaussian 16 Rev. C.01*, Wallingford, CT, 2016.

41.   Paquette, L. A.; Beckley, R. S.; Farnham, W. B., Silver(I) ion catalyzed rearrangements of strained .sigma. bonds. XXVII. Kinetic analysis of the silver(I)-catalyzed 1,8-bishomocubane-snoutane rearrangement. *J. Am. Chem. Soc.* **1975,** *97* (5), 1089-1100.

42.   Bishop, K. C., Transition metal catalyzed rearrangements of small ring organic molecules. *Chem. Rev.* **1976,** *76* (4), 461-486.

43.   Elkoush, T.; Reich, N. D.; Campbell, M. G., Dinuclear Silver Complexes in Catalysis. *Angew. Chem. Int. Ed. Engl.* **2021,** *60* (42), 22614-22622.

44.   Scholz, F.; Himmel, D.; Heinemann, F. W.; Schleyer, P. v. R.; Meyer, K.; Krossing, I., Crystal Structure Determination of the Nonclassical 2-Norbornyl Cation. *Science* **2013,** *341* (6141), 62-64.

cubanes   cuneanes

- Regioselectivity
- Post-isomerization functionalization
- Mechanism study
- Molecular dynamics